Research Article

Structural, elastic and thermo-physical properties of Er_2O_3 nanoparticles doped bio-silicate borotellurite glasses

S. A. Umar[1,2] · M. K. Halimah[2] · M. N. Azlan[3] · L. U. Grema[4] · G. G. Ibrahim[2,6] · A. F. Ahmad[2] · A. M. Hamza[2,5] · M. M. Dihom[2,7]

Received: 10 December 2019 / Accepted: 27 January 2020 / Published online: 30 January 2020

Abstract

This paper presents a study on the structural, morphological and elastic properties of erbium oxide nanoparticles doped bio-silicate borotellurite glass system fabricated using the technique of melt-quenching with chemical compositional formula $\{[(TeO_2)_{0.7}\ (B_2O_3)_{0.3}]_{0.8}\ (SiO_2)_{0.2}\}_{1-y}\ (Er_2O_3\ NPs)_y$ where $0.01 \le y \le 0.05$. The objective of the work was to study the some elastic and thermal parameters associated with non-destructive ultrasonic technique, with the aim of utilizing the glasses for erbium doped fiber amplifier application. Various measurements and Characterizations techniques which includes density and molar volume measurements, energy dispersive X-ray fluorescence, X-ray diffraction (XRD), Fourier transform infrared (FTIR), Transmission electron microscopy and Pulse-echo technique were carried out in this study. The density values for the glasses increased from 4.1900 to 4.6003 gcm^{-3} with the addition of 1–5% of Er_2O_3 NPs in the glass structure. The increase can be ascribed to increase in the overall molar weight of the glass due to incorporation of heavy Er^{3+} ions. The XRD patterns revealed no presence of sharp peaks with the observed broad hump around $2\theta = 20–30°$ indicating the glassy and amorphous nature of the studied glasses. The FTIR spectra showed absorption with peaks around 1362–1385 cm^{-1}, 1221–1250 cm^{-1}, 655–689 cm^{-1} and 602–630 cm^{-1} wave number ranges, indicating the presences of H_3BO_3, SiO_4, BO_3, TeO_3 and TeO_4 structural units in the glass system. The microstructural nature observed in the glass morphology showed nanoparticle agglomerations in the glasses. The ultrasonic velocities, elastic moduli, microhardness, Poisson ratio, softening and Debye's temperatures, thermal expansion coefficient as well as other important parameters were calculated from the density and ultrasonic data. The values of the ultrasonic velocities, elastic moduli, Debye's temperature, softening temperature, thermal expansion coefficient and the acoustic impedance increased with increase in the Er_2O_3 NPs concentration.

Keywords Rice husk silica · Er_2O_3 NPs · XRD · FTIR · Ultrasonic technique · Elastic moduli

✉ S. A. Umar, usaltilde@yahoo.com; M. K. Halimah, halimahmk@upm.edu.my; M. N. Azlan, azlanmn@fsmt.upsi.edu.my; L. U. Grema, lawangrema@yahoo.com; G. G. Ibrahim, ibgana55@gmail.com; A. F. Ahmad, ahmad_al67@yahoo.com; A. M. Hamza, amhamza419@gmail.com; M. M. Dihom, mdihom71@gmail.com | [1]Department of Physics, Faculty of Science, Federal University Lafia, Lafia, Nasarawa State, Nigeria. [2]Department of Physics, Faculty of Science, Universiti Putra Malaysia, 43400 UPM Serdang, Selangor, Malaysia. [3]Physics Department, Faculty of Science and Mathematics, Universiti Pendidikan Sultan Idris, 35900 Tanjung Malim, Perak, Malaysia. [4]Department of Mechanical Engineering, Ramat Polytechnic Maiduguri, Maiduguri, Borno State, Nigeria. [5]National Agency for Science and Engineering Infrastructure, Abuja, Nigeria. [6]Department of Physics, Yobe State University, Damaturu, Nigeria. [7]Department of Physics, Al Asmarya Islamic University, Zliten, Libya.

SN Applied Sciences (2020) 2:291 | https://doi.org/10.1007/s42452-020-2112-x

1 Introduction

In the last few decades, the need for an increased rice husk commercialization is ever increasing with continued increase in the global rice production above 645 million tonnes annually [1]. The commercialization of the rice milling waste beyond the present 30% becomes necessary so as to solve the environmental pollution problems caused by their continued disposal and also help in solving some the mankind's problems [1, 2]. One of the areas considered these days for the rice husk is in glass and ceramics fabrications for optical fibre, optoelectronics and other glass and ceramics technological applications [3–5]. Many different researchers have worked on the silicate extraction (from the rice husk) for fabrication different glass compositions for various technological and industrial applications [6, 7].

Glass science and technology research in the present days has been giving great attention to the fabrications and utilizations TeO_2-based glasses [8]. Tellurium oxide based glasses have demonstrated more advantages over other silicate and phosphate glasses due to their low melting point, high rare RE ions solubility, high effect of stark splitting, high refractive index and high optical transparency in wide spectral region [9–11]. Tellurium oxide alone does not form glass on its own, but rather require combination with other glass formers or modifiers. TeO_2–B_2O_3 combination was found to be one of the most favourable combinations for the glass utilization in the area of optical fibre amplifiers, optoelectronics and laser applications [5, 9]. Borotellurite glasses presents a compromising quality against the individual disadvantages of B_2O_3 and TeO_2 by having high chemical durability, high refractive index, high thermal stability, low melting point, and high refractive index [12].

Among the number of rare earth (RE) ions used in the areas of optical fibres, optoelectronic and lasers, Er^{3+} ions are found to be more suitable for optical signal amplifiers and sometimes laser applications and white-light emitting devices [13]. Since Er^{3+} ions in glasses possesses two useful emission bands around 1500 nm and 2700 nm, the former is utilized in the EDFA and the 2700 nm band is utilized in medicine and optical sources for sensors [14]. The area of optical transmission in the communication system requires gain bandwidth widening of the optical amplifiers that is utilized in the wavelength division multiplexing (WDM) systems [15].

Non-destructive ultrasonic technique have been used various researchers in the study of elastic properties of non-crystalline and crystalline materials alike [16]. The ultrasonic velocities were used together with density and their molecular/structural data for the calculation of the elastic moduli, microhardness, acoustic impedance, softening temperature, Debye temperature, fractal bond connectivity and the Poisson ratio [16, 17]. In another study, the elastic properties of erbium oxide doped TeO_2–ZnO–P_2O_5–$LiNbO_3$ was reported. The elastic moduli investigated was found to have increased with Er^{3+} ions concentration increased [18].

In this study a choice was made for SiO_2–TeO_2–B_2O_3 composition for erbium oxide nanoparticles' hosting with the aim of increasing the rice husk commercialization (through SiO_2 extraction) in the area of lasers and EDFA applications. The choice of TeO_2 was to improve the refractive index and the optical transparency in the IR region. B_2O_3 was selected to compromise the high phonon energy of the TeO_2, lower the glass forming temperature, improve the RE solubility and hardness [19]. SiO_2 composition aimed at improving both the thermal and chemical stability as well as the mechanical strength of the glasses [2].

Non-destructive ultrasonic technique was employed in this work for the collection of ultrasonic velocity data. The elastic moduli, Poisson ratio, micro-hardness, Debye temperature, softening temperature, acoustic impedance, thermal expansion coefficient and fractal bond connectivity as well as the morphological and structural properties were studied. The ultrasonic studies provides information on glass structure as well as some thermal and mechanical features of studied glasses [16, 20]. For better utilization of glass material in the EDFA and laser applications, studying the elastic properties of such material is very important especially as some glasses' elastic properties might not always favour fibre drawing.

1.1 Experiments

From rice milling factory in Malaysia, rice husk (rice milling waste) was obtained. Using the simple cold acid (HCl) leaching technique, 98.548% of SiO_2 was extracted. The extracted SiO_2 was used with Er_2O_3 NPs (Alfar Aeser, 99.9%), B_2O_3 (Alfar Aeser, 99.9%) and TeO_2 (Alfar Aeser, 99.9%) for the fabrication of $\{[(TeO_2)_{0.7}\ (B_2O_3)_{0.3}]_{0.8}\ (SiO_2)_{0.2}\}_{1-y}\ (Er_2O_3\ NPs)_y$ using melt-quenching technique.

For the glass fabrication, powdered chemicals were weighed using electronic weighing balance in accordance with the compositional chemical equation. The weighed chemicals were made homogeneous by stirring for ½ hour in an alumina crucible. The crucible containing the homogeneous mixture is then put into a 400 °C electric furnace for 1 h preheating before transferring to another furnace at around 900 °C for another 2 h for mixture melting. The preheating was necessary to enable the evaporation of any possible moisture in the mixture as B_2O_3 is highly hygroscopic in nature [10]. The molten material was turned into a cylindrical molt and transferred to the 400 °C furnace for

1 h annealing to remove thermal stress and bubbles before being allowed to cool down to room temperature [9]. The cylindrical glasses were finally cut to about 4–5 mm thickness for non-destructive ultrasonic probing and the remaining portion grinded for XRD, TEM and FTIR analyses.

The XRF analysis of the extracted SiO_2 was performed using the Energy Dispersive X-ray Spectrometer (Shimadzu model EDX-720) to determine its purity. The density was measured using MD-300S, Alfa Mirage electronic densimeter and using the Archimedes principle. Using Archimedes principle, the glass density (ρ) and molar volume (V_m) were calculated as follows;

$$\rho = \frac{W_{Air}}{W_{water}} \quad (1)$$

$$V_m = \frac{M_w}{\rho} \quad (2)$$

where water density was taken to be 1 g/cm^3, M_w = molecular weight of glass, W_{air} = weight of sample in air, and W_{water} = sample weight in water [9].

Other characterization performed includes the X-ray diffraction (XRD) using the XRD system {PANalytical (Philips) PW3050/60}, Fourier transform infrared (FTIR) using Perkin Elmer 1650 spectrometer and Transmission Electron Microscopy (TEM) using JOEL transmission electron microscope that operates at 200 kV. Using Ritec Ram-5000 Snap System, ultrasonic pulse-echo technique was performed to determine the ultrasonic (longitudinal and shear) velocities in the samples.

1.2 Results and discussions

Table 1 presents the XRF analysis result of the SiO_2 extracted from rice husk using cold HCl leaching method. Unlike the hot leaching technique presented by Mustapha et al. [21] which requires heating, the present SiO_2 extraction require no heating during leaching and is cost effective as well. About 98.548% pure SiO_2 was achieved as shown in Table 1.

Table 1 Result of the XRF analysis of rice husk extracted SiO_2

Element (Oxide)	Amount/Percentage (%)
SiO_2	98.548
SO_3	0.793
CaO	0.407
Fe_2O_3	0.129
K_2O	0.079
MnO	0.035
ZnO	0.009

The XRD patterns for the studied glasses are presented in Fig. 1. XRD result study is used for identification of amorphous nature and crystalline phase presences in samples [22]. The patterns in Fig. 1 showed the spectra recorded between $20° \le 2\theta \le 80°$ observed at lower scattering angles is a broad diffusion indicating the presence of long range structural disorder in the glasses [23]. The presence of a broad hump around $2\theta = 27°$ indicates the glassy/amorphous nature of the studied glasses. As observed in the Figure, as the Er_2O_3 NPs are increased in concentration, the broad hump continue to narrow, suggesting the tendency of crystallization with continued increase in the Er_2O_3 NPs concentration [24].

The density and molar volume variation with Er_2O_3 NPs concentration is presented in Fig. 2. The density value increased from 4.1900 to 4.6004 gcm^{-3} as the concentration of Er_2O_3 NPs increased from 0.01 to 0.05 Molar. The high density value observed might be due to the high material compactness resulting from to the presence of nanoparticle of Er_2O_3. The increase in the density value with dopant increase might be associated to decrease in the non-bridging oxygen number which can be confirmed

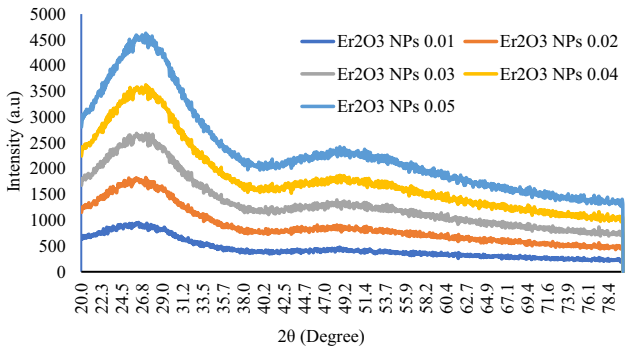

Fig. 1 XRD patterns of the $\{[(TeO_2)_{0.7}\ (B_2O_3)_{0.3}]_{0.8}\ (SiO_2)_{0.2}\}_{1-y}\ (Er_2O_3\ NPs)_y$ glass system

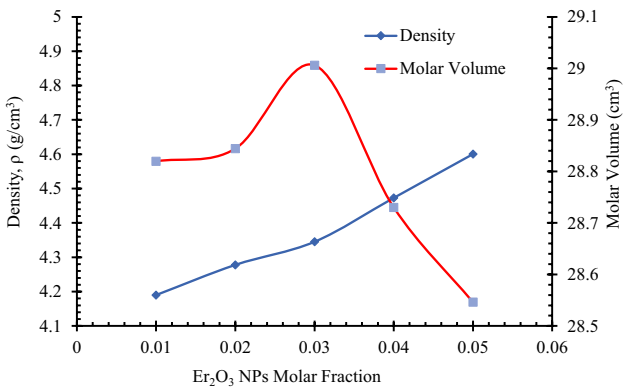

Fig. 2 Density and molar volume $\{[(TeO_2)_{0.7}\ (B_2O_3)_{0.3}]_{0.8}\ (SiO_2)_{0.2}\}_{1-y}$ $(Er_2O_3\ NPs)_y$ glass system

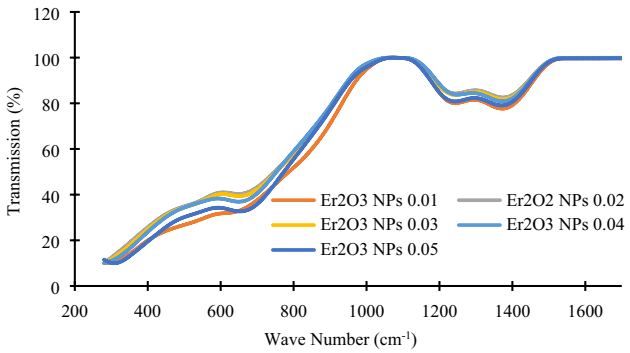

Fig. 3 FTIR Spectra of $\{[(TeO_2)_{0.7}\ (B_2O_3)_{0.3}]_{0.8}\ (SiO_2)_{0.2}\}_{1-y}\ (Er_2O_3\ NPs)_y$ glass system

by the TeO_4/TeO_3 concentration variations in Fig. 4. The increase in the density might also be due to increased substitution of lighter B^{3+}, Si^{4+},and Te^{4+} ions with comparatively much heavier ions of Er^{3+}, resulting in the overall glass molecular weight increase [19]. The molar volume increased from 28.8196 to 29.0061 cm^3 and then decreased down to 28.6456 cm^3 as the dopant's concentration raised from 0.01 to 0.03 and down to 0.05 M respectively. The initial value increase can be attributed to a decrease in atomic compactness in the glasses network due to breakage one of the double bonds of oxygen atoms in the network (decreased connectivity) resulting from the formation of TeO_3 structural units [9]. The decrease in the glasses' molar volume with addition of more dopant can be due the increase in the concentration TeO_4 units suggesting more cross-linkage between the oxygen atoms and the cations in the glass network [17].

The FTIR spectra for the studied Er_2O_3 NPs doped silica borotellurite glasses are presented in Fig. 3. Various IR peak positions observed and recorded include the absorption peaks around wave number range of 602–630 cm^{-1}, 655–689 cm^{-1}, 950–1150 cm^{-1}, 1221–1250 cm^{-1} and 1362–1385 cm^{-1}. The assignment of each absorption peak is presented in Table 2.

Table 3 and Fig. 4 present the variation of the trigonal pyramidal (TeO_3) and trigonal bipyramidal (TeO_4) structural units against the Er_2O_3 NPs molar concentration.

Table 3 Relative areas of the peaks deconvoluted for the study of FTIR spectra of the $\{[(TeO_2)_{0.7}\ (B_2O_3)_{0.3}]_{0.8}\ (SiO_2)_{0.2}\}_{1-y}\ (Er_2O_3\ NPs)_y$ glasses

Y	TeO_4	TeO_3	BO_3	$B\Theta_3/B\Theta_2O$
0.01	784	113	9.5	17.458
0.02	748.75	128.62	7.9421	12.851
0.03	800.12	126.6	8.422	13.573
0.04	898.9	117.84	8.67	13.879
0.05	988.5	83.68	10.277	15.084

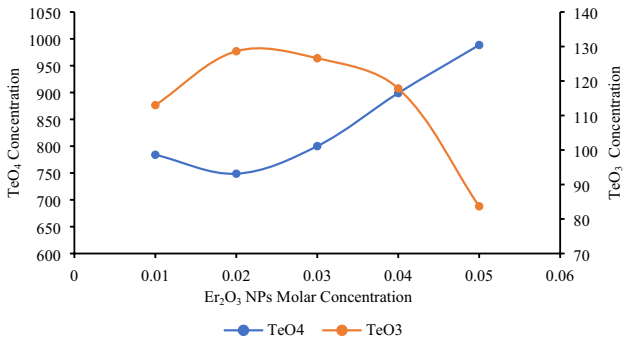

Fig. 4 Variation of concentration of TeO_3 and TeO_4 structural units with molar fraction Er_2O_3 NPs in $\{[(TeO_2)_{0.7}\ (B_2O_3)_{0.3}]_{0.8}\ (SiO_2)_{0.2}\}_{1-y}\ (Er_2O_3\ NPs)_y$ glass system

Increase in the TeO_4 concentration is associated with increase in oxygen atoms bonding in the glass network while the TeO_3 concentration increase relates to the increase in the oxygen atoms bond breakage. BO3 concentration presented in Table 2 is from the area under the curve around 1221 cm^{-1} and 12,250 cm^{-1} [26]. While the increase in the $B\Theta_3$ concentration represents the area under the curve around 1362–1385 cm^{-1} [27]. Thus, with TeO_4 concentration increase we have more bridging oxygen atoms created and TeO_3 creates more non-bridging oxygen atoms in the glass network [28].

The TEM microstructure of the studies Er_2O_3 NPs doped rice husk silicate borotellurite glass system is presented in Fig. 5. Er_2O_3 NPs of various sizes can be observed in the

Table 2 FTIR spectral peak assignment for $\{[(TeO_2)_{0.7}\ (B_2O_3)_{0.3}]_{0.8}\ (SiO_2)_{0.2}\}_{1-y}\ (Er_2O_3\ NPs)_y$ glass system

Position of FTIR peak (cm^{-1})	Assignment of IR
602–630	Te–O bond vibrations between the trigonal bipyramid unit (TeO_4) and the bridging oxygen atom [9]
655–689	Te–O bond asymmetric vibrations in the TeO_3 units [5]
950–1150	Si–O–Si asymmetric stretching of the bridging oxygen atoms of silica [2]. The peak position might also be attributed to B–O stretching vibration in BO_4 structural unit [8]
1221–1250	Stretching vibrations of B–O in the BO_3 units in boroxol rings [19]
1362–1385	Asymmetric stretching modes of borate triangles $B\Theta_3$, $B\Theta_2O$ with NBO [25]

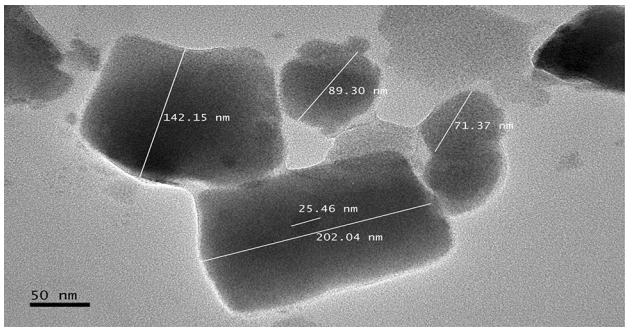

Fig. 5 TEM micrograph of $\{[(TeO_2)_{0.7}\ (B_2O_3)_{0.3}]_{0.8}\ (SiO_2)_{0.2}\}_{1-y}$ $(Er_2O_3$ NPs$)_y$ glass with 3% Er_2O_3 NPs

diagram with lager particles of micro-sizes. The larger particles might have formed from the fusion of small nanoparticles through Oswald ripening effect in the glass network, which happened after the formation of glass [28].

The values of the ultrasonic velocities of the system of Erbium NPs doped RHSBT glasses were presented in Table 4. The ultrasonic wave velocities were calculated as;

$$v = \frac{2x}{t} \tag{3}$$

$$v_m = \left(\frac{v_L^3 + v_s^3}{3}\right)^{\frac{-1}{3}} \tag{4}$$

where v is the longitudinal (V_L) or shear (V_s) velocity, t is time of travel of the ultrasonic wave to and fro inside the glass sample and x is the sample thickness and v_m is the mean ultrasonic velocity [29]. The longitudinal, shear and the mean ultrasonic velocities for the studied glasses increased from 3722.15 to 4087.26 m/s, 2214.38 to 2345.19 m/s and 2994.21 to 3190.21 m/s respectively as Er_2O_3 NPs concentration was increased 1–5% molar composition. The velocities are directly related to the material density and hence increase in material density may cause an increase in the values of the ultrasonic velocities [30]. The increase in the values may also be associated with the increased compactness in the glass network which resulted from increase in the number of bridging oxygen (BO) in the network [31].

Table 4 and Fig. 6 present the elastic moduli of the Erbium NPs doped RHSBT glasses. The elastic [Longitudinal (L), Shear (G), Young (E) and Bulk (K)] moduli were calculated using the data of density (ρ), longitudinal (V_L) and Shear (V_s) velocities as reported by [17] as;

$$G = V_s^2 \rho \tag{5}$$

$$L = V_L^2 \rho \tag{6}$$

$$K = L - \frac{4}{3}G \tag{7}$$

$$E = (1 - \sigma)2G \tag{8}$$

The longitudinal, shear, young and bulk moduli increased from 58.050 to 76.853 GPa, 20.546 to 25.302 GPa, 31.801 to 37.720 GPa and 30.656 to 43.117 GPa respectively. The increase in the elastic moduli has a connection to the fact that the material connectivity in the glass system increased with the increase in Er_2O_3 NPs content. This is due to the formation of more TeO_4 units in the glass network which suggests a decrease in the formation of NBO

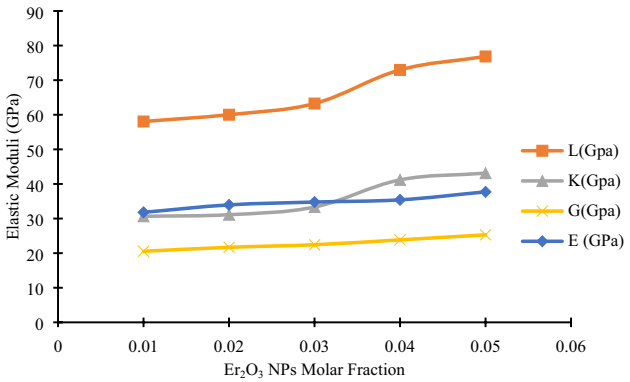

Fig. 6 Elastic moduli variation with molar fraction of Er_2O_3 NPs in $\{[(TeO_2)_{0.7}\ (B_2O_3)_{0.3}]_{0.8}\ (SiO_2)_{0.2}\}_{1-y}$ $(Er_2O_3$ NPs$)_y$ glass system

Table 4 Longitudinal Velocity (V_L, ms^{-1}), Shear Velocity (V_S, ms^{-1}), Mean Velocity (V_m, ms^{-1}), Longitudinal Modulus (L, GPa), Shear Modulus (G, GPa), Bulk Modulus (K, GPa) and Young Modulus (E, GPa) of Er_2O_3 NPs in $\{[(TeO_2)_{0.7}\ (B_2O_3)_{0.3}]_{0.8}\ (SiO_2)_{0.2}\}_{1-y}$ $(Er_2O_3$ NPs$)_y$ Glass System

Y	V_L (m/s)	V_S (m/s)	V_m (m/s)	L (GPa)	G (GPa)	K (GPa)	E (GPa)
0.01	3722.15	2214.38	2994.21	58.050	20.546	30.656	31.801
0.02	3745.94	2251.51	3038.92	60.026	21.685	31.112	33.951
0.03	3815.30	2272.34	3071.98	63.249	22.436	33.335	34.770
0.04	4038.99	2308.72	3142.49	72.969	23.842	41.180	35.412
0.05	4087.26	2345.19	3190.21	76.853	25.302	43.117	37.720

and hence more rigid network formation [32, 33]. The elastic moduli increase might also result from the increase in the overall stretching force constant of the glasses. This might be attributed to the modifier role of the Er^{3+} ions in the glass network. The Er^{3+} ions increase can cause an increase in the coulomb contribution to the lattice energy in the glass system [34].

The micro-hardness and fractal bond connectivity values for different Nano Er_2O_3 concentrations in the Nano Erbium Doped RHSBT Glass System are presented in Fig. 7 and Table 5. The micro-hardness (*H*), Poisson (σ) and the fractal bond connectivity (*d*) were calculated as follows;

$$d = 4G/K \tag{9}$$

$$\sigma = \frac{(L - 2G)}{2(L - G)} \tag{10}$$

$$H = \frac{(1 - 2\sigma)E}{6(1 + \sigma)} \tag{11}$$

The variation in the micro-hardness as can be observed shows direct proportionality with the fractal bond connectivity in Fig. 7 and inverse proportionality with the Poisson ration in Fig. 8. By definition, micro-hardness refers to material's resistance to penetration or indentation [29]. The increase observed in the micro-hardness value is an indication of an increased rigidity and network connectivity in the glasses and the decrease indicates the opposite [17]. The fractal bond connectivity value changed from 2.6808 to 2.7880 and then to 2.3472 as the Nano Er_2O_3 concentrations increased from 1 to 5% in the glass network. This is an indication of the structural change from tetrahedral structure (3D) to a 2D layer or structure [29].

The Poisson's ratio of a material gives a measure of the resistance of the material to volume change as well as to shape change. It can also be defined as the negative of the ratio of contraction of transverse strain to extension of longitudinal strain in the applied force direction [35, 36]. Poisson's ratio is small for shear resistant but compressible materials such as cellular solids and can reach 0.5 for incompressible bodies such as rubber. Glasses fall in between these two and have values from 0.1 to 0.4 and specifically for oxide glasses mainly in the 0.16–0.3 with highly polymerized silica rich glass having the lowest value of theoretical volume occupied (V) and the highest for glass networks consisting of chains and cluster units [37].

Table 5 Micro-hardness (H), Poisson Ratio (σ), Softening Temperature (T_S), Fractal Bond Connectivity (d) Values for Er_2O_3 NPs in $\{[(TeO_2)_{0.7}\ (B_2O_3)_{0.3}]_{0.8}\ (SiO_2)_{0.2}\}_{1-y}\ (Er_2O_3\ NPs)_y$ Glass System

Y	H (GPa)	σ	T_S (K)	θ_D (K)	D
0.01	2.3681	0.2261	1046.78	536.984	2.6808
0.02	2.6293	0.2172	1083.11	545.957	2.7880
0.03	2.6002	0.2251	1109.43	552.973	2.6922
0.04	2.2780	0.2573	1135.87	566.605	2.3158
0.05	2.4594	0.2546	1162.97	576.050	2.3473

The Poisson ratio relation with the concentration of Er_2O_3 NPs in an erbium NPs doped RHBT glass system is presented in Fig. 8. The relation showed a decrease in the value from 0.22609 to 0.217202 as the Er_2O_3 NPs molar concentration increased from 1 to 2%. The value then increased to 0.257384 when the Er_2O_3 NPs molar concentration was increased to 4% which the decreased to 0.25459 when the Er_2O_3 NPs molar concentration reached 5%. The decrease in the Poisson's ratio value with increase in Er_2O_3 NPs molar concentration may be due to an increase in the glass ionicity which is caused by more polar bonding presence in the modifiers [34]. The increase in the Poisson ratio may be associated to increase in the crosslink density in the glass network [38].

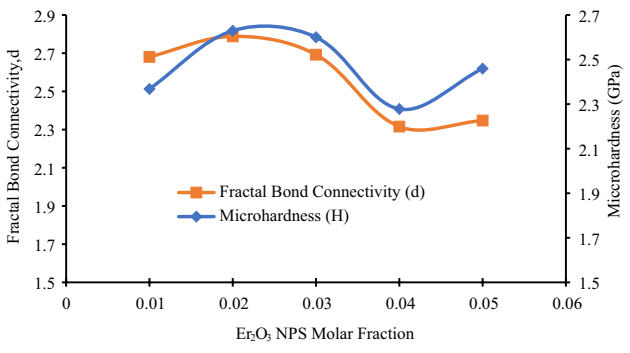

Fig. 7 Micro-hardness and fractal bond connectivity variation with molar fraction of Er_2O_3 NPs in $\{[(TeO_2)_{0.7}\ (B_2O_3)_{0.3}]_{0.8}\ (SiO_2)_{0.2}\}_{1-y}\ (Er_2O_3\ NPs)_y$ glass system

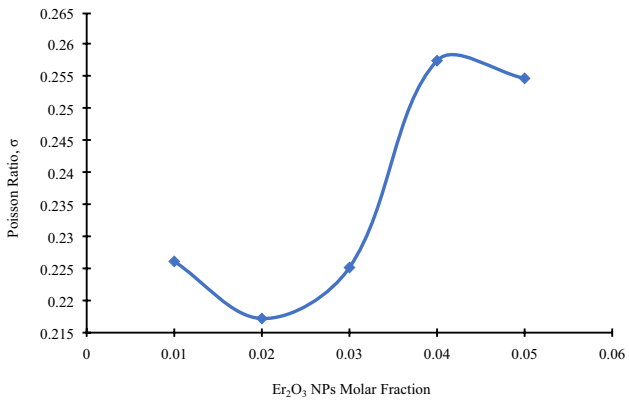

Fig. 8 Poisson ratio variation with molar fraction of Er_2O_3 NPs in $\{[(TeO_2)_{0.7}\ (B_2O_3)_{0.3}]_{0.8}\ (SiO_2)_{0.2}\}_{1-y}\ (Er_2O_3\ NPs)_y$ GLASS system

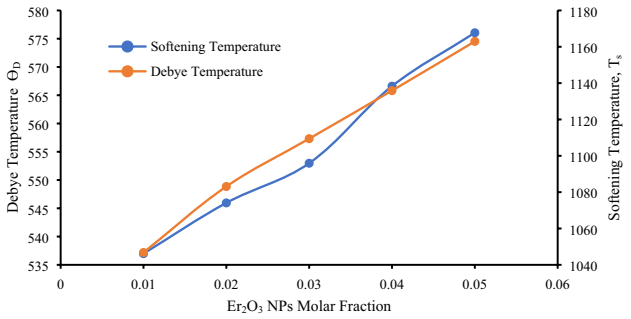

Fig. 9 Softening temperature and Debye temperature variation with Er_2O_3 NPs molar fraction in $\{[(TeO_2)_{0.7}\ (B_2O_3)_{0.3}]_{0.8}\ (SiO_2)_{0.2}\}_{1-y}$ $(Er_2O_3\ NPs)_y$ glass system

The Debye and softening temperatures' variation with concentration of Er_2O_3 NPs are presented in Fig. 9 and Table 5. The softening temperature (T_s) and the Debye temperature (θ_D) were calculated using the following standard relations as follows;

$$T_s = \frac{M_w}{c\rho} V_s^2 \tag{12}$$

$$\theta_D = \frac{h}{k}\left[\frac{9PNa}{4\pi}\right]^{\frac{1}{3}} v_m \tag{13}$$

where M_w is the glass molecular weight, v_m is the mean ultrasonic velocity, h is the Plank's constant, P is the number of atoms in the chemical formula, k is the Boltzmann constant, $c = 1.35 \times 10^9\ cm^5\ K^{-1}s$ is constant, N_a is the Avogadro's number, ρ is the density of the given sample and V_s is the ultrasonic shear velocity inside the glass [17, 18].

As the concentration of Er_2O_3 NPs increased from 1 to 5% in the glass system, the values of the softening temperature and Debye temperature increased from 1046.78 to 1162.97 K and 536.984 to 576.050 K respectively. Debye temperature provides the description properties related to atomic vibrations in a solid material; it represents the excitation temperature of high frequency lattice in any material understudy. In glassy materials, network vibrational spectrum are considered as a diffuse version of the lattice spectrum of the equivalent crystal nearest to it [39]. The increase in the value of the Debye temperature recorded can be ascribed to stronger packing and increase connectivity in the glass system arising from more bonding of single bonded oxygen atoms as well as increased lattice vibrations in the glass network [40]. Whereas the softening temperature represents the temperature at which viscous flow translates to plastic flow in a material. The increase in T_s value with Er_2O_3 NPs composition increase might be associated with increase in the rigidity and connectivity because of increased connectivity. The increased connectivity might as well be attributed to the observed TeO_4 concentration increase and TeO_3 concentration decrease in the glass structure, which signifies more bonding of oxygen atoms in the glasses [17].

The variation of thermal expansion coefficient (α_p) and acoustic impedance (Z) with Er_2O_3 NPs concentration is presented in Fig. 10 and Table 6. The acoustic impedance and the thermal expansion coefficient were determined from the longitudinal ultrasonic data using the following expressions as reported by Marzouk and Gafaar [31] as follows;

$$Z = V_L \rho \tag{14}$$

$$\alpha_P = 23.2\left(V_L - 0.57457\right) \tag{15}$$

In glasses, the thermal expansion coefficient value and its transition temperature are interdependent. The value is also dependent on other parameters which includes the composition and nature of glass modifier, temperature region as well as thermal history of the glasses [41]. The increase in the linear thermal expansion coefficient represents a decrease in the thermal stability of the glasses with increase in Er_2O_3 NPs composition [42]. Acoustic impedance is a parameter responsible for both reflection and transmission of sound energy inside a material [31]. Increase in the value recorded for the studied glass system can be ascribed to atomic compactness and glass network rigidity [43].

The variation of the fugacity value with Er_2O_3 NPs molar concentration is presented in Fig. 11. This is the proportion of free volume at the temperature of glass transition. The variation in the fugacity as shown in the figure indicates increase and then a decrease in the value. This is because of an interstitial space increase in the beginning with increase in the Er_2O_3 NPs molar concentration resulting from the formation of more NBOs. The decrease in the

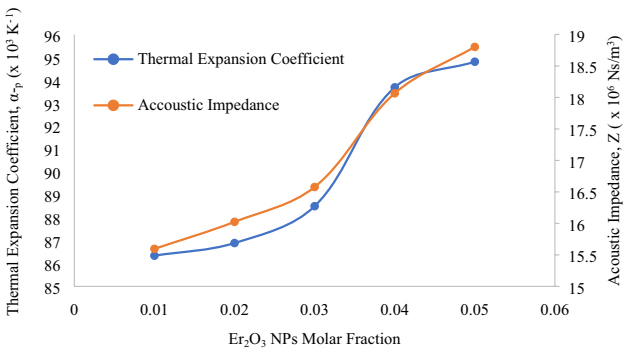

Fig. 10 Acoustic impedance and thermal expansion coefficient variations with Er_2O_3 NPs molar fraction in $\{[(TeO_2)_{0.7}\ (B_2O_3)_{0.3}]_{0.8}\ (SiO_2)_{0.2}\}_{1-y}$ $(Er_2O_3\ NPs)_y$ glass system

Table 6 Fugacity (f_g), Acoustic Impedance (Z), Thermal Expansion Coefficient (α_p), Diffusion Constant (D_i), Latent Heat of Melting (ΔH_m) values for different Er_2O_3 NPs Molar Fraction in $\{[(TeO_2)_{0.7}\ (B_2O_3)_{0.3}]_{0.8}\ (SiO_2)_{0.2}\}_{1-y}\ (Er_2O_3\ NPs)_y$ Glass System

y	f_g	$Z\ (\times 10^6\ Ns/m^3)$	$\alpha_p\ (\times 10^3\ K^{-1})$	$D_i\ (\times 10^{-9}\ m^{-2}\ s^{-1})$	ΔH_m (J)
0.01	0.1939	15.5958	86.3406	3.3412	33,395.71516
0.02	0.2043	16.0244	86.8925	3.6816	35,466.82031
0.03	0.1950	16.5779	88.5016	3.7635	37,366.15985
0.04	0.1586	18.0660	93.6913	3.8325	40,271.45791
0.05	0.1616	18.8030	94.8111	3.9482	42,710.3687

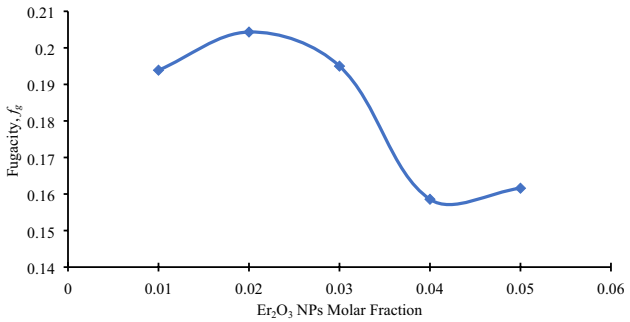

Fig. 11 Variation of fugacity with molar fraction of Er_2O_3 NPs in $\{[(TeO_2)_{0.7}\ (B_2O_3)_{0.3}]_{0.8}\ (SiO_2)_{0.2}\}_{1-y}\ (Er_2O_3\ NPs)_y$ glass system

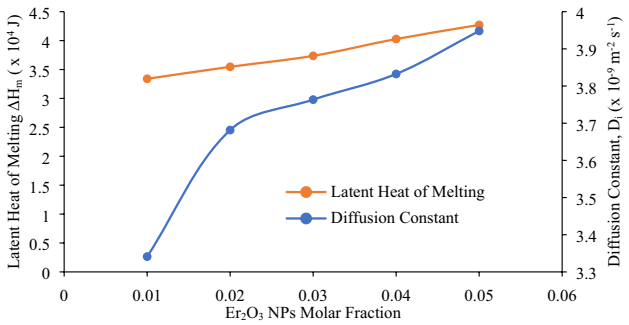

Fig. 12 Latent heat of melting and diffusion constant variation with molar fraction of Er_2O_3 NPs in $\{[(TeO_2)_{0.7}\ (B_2O_3)_{0.3}]_{0.8}\ (SiO_2)_{0.2}\}_{1-y}\ (Er_2O_3\ NPs)_y$ glass system

value afterwards indicates an increase in material compactness as the Er_2O_3 NPs molar concentration is increase. The decrease in the fugacity may as well be considered to be due to an increase in the concentration of bridging oxygen (BO) in the glass network [44]. This parameter also related to the Poisson ratio and is a factor of material permeability in the glass network [45].

The calculations of the latent heat of melting (ΔH_m) and the diffusion constant (D_i) were carried out using the expressions as reported by Chinnamat et al. [29], as presented in Eqs. (16) and (17) as follows;

$$\Delta H_m = \frac{9M\theta_D^2 r_i^2 k_B^2}{128h^2} \tag{16}$$

$$D_i = \frac{k_B \theta_D r_i^2}{96h} \tag{17}$$

The Variation of diffusion constant and latent heat of melting with concentration of Er_2O_3 NPs in the studied glass system is presented in Fig. 12. The diffusion constant value for the studied glasses increased from 3.3412×10^{-9} to $3.9482 \times 10^{-9}\ m^{-2}\ s^{-1}$ when the concentration of Er_2O_3 NPs was increased from 1 to 5 mol%. The increase in the value might be connected to increase in the ionic bond length resulting from the substitution of other oxides with shorter bond length with longer bonds of Er_2O_3 NPs, making the overall bond length of the glasses longer [29]. The increase might also be connected to increase in the number of vibrating atoms in the glass network [31]. The latent heat of melting increased in value from 33.397 to 42.7104 kJ as the Er_2O_3 NPs composition increased from 1 to 5 mol%. Increase in the value together with increase in the diffusion constant confirmed the increase in the Debye's and softening temperatures [31, 46].

2 Conclusion

Using the agricultural waste (rice husk), silica was extracted with 98.584% purity and was used in the fabrication of a system of erbium doped silica borotellurite glasses with chemical composition $\{[(TeO_2)_{0.7}\ (B_2O_3)_{0.3}]_{0.8}\ (SiO_2)_{0.2}\}_{1-y}\ (Er_2O_3\ NPs)_y$ using the method of melt-quenching. The aim was to improve the rice husk commercialization from its current 30% in the area of Erbium doped fiber amplifier technology. The glasses were subjected to various measurements and characterizations which include density and molar volume, EDX, XRD, TEM, FTIR and the pulse-echo non-destructive ultrasonic technique for the study of the glasses' structural and elastic properties. The measured density values increased from 4.1900 to 4.6004 gcm^{-3} and the XRD patterns revealed the amorphous nature of the glasses. FTIR spectral study showed the presence of TeO_4, TeO_3, SiO_4, H_2BO_3, and two different structural units of

BO_3, with the TEM revealing the presence of Er_2O_3 NPs and larger particles of agglomerated NPs of Er_2O_3 were formed through Oswald ripening effect. The ultrasonic velocities as well as elastic moduli increased with increased Er_2O_3 NPs concentration. The microhardness, softening temperature, Debye temperature, thermal expansion coefficient, acoustic impedance, diffusion constant, fractal bond connectivity, fugacity as well as the latent heat of melting were determined for the studied glasses. Based on the studied parameters, the glasses proved to be strong enough to stand fiber drawing and thermal stress.

Acknowledgement The authors appreciate the financial support for the work from the Minister of Higher Education of Malaysia and University Putra Malaysia through grant Putra Berimpak 9597200.

Compliance with ethical standards

Conflict of interest The authors wish to state that there is no conflict of interest whatsoever in this work and all authors who contributed to the development of this article have been listed and financial contributors duly acknowledged.

References

1. Prasad R, Pandey M (2012) Rice husk ash as a renewable source for the production of value added silica gel and its application: an overview. Bull Chem React Eng Catal 7(1):1–25. https://doi.org/10.9767/bcrec.7.1.1216.1-25
2. Umar SA, Halimah MK, Hamza AM, Abdulbaset AA (2018) The structural, physical and optical properties of borotellurite glasses incorporated with silica from rice husk. J Sci Math Lett 6:32–46
3. Kaewkhao J, Limsuwan P (2012) Utilization of rice husk fly ash in the color glass production. Proc Eng 32(32):670–675. https://doi.org/10.1016/j.proeng.2012.01.1325
4. Lee CS, Matori KA, Ab Aziz SH, Kamari HM, Ismail I, Zaid MHM (2017) Fabrication and characterization of glass and glass-ceramic from rice husk ash as a potent material for opto-electronic applications. J Mater Sci Mater Electron 28(23):17611–17621. https://doi.org/10.1007/s10854-017-7699-3
5. Umar SAA, Halimah MKK, Chan KTT, Latif AAA (2017) Physical, structural and optical properties of erbium doped rice husk silicate borotellurite (Er-doped RHSBT) glasses. J Non Cryst Solids 472:31–38. https://doi.org/10.1016/j.jnoncrysol.2017.07.013
6. Hamza AM, Halimah MK, Muhammad FD, Chan KT (2019) Physical properties, ligand field and Judd-Ofelt intensity parameters of bio- silicate borotellurite glass system doped with erbium oxide. J Lumin 207:497–506. https://doi.org/10.1016/j.jlumin.2018.11.038
7. Mohanta K, Kumar D, Parkash O (2012) Properties and industrial applications of rice husk: a review. Int J Emerg Technol Adv Eng 2(10):86–90
8. Halimah MK et al (2019) Effect of erbium nanoparticles on structural and spectroscopic properties of bio-silica borotellurite glasses containing silver oxide. Mater Chem Phys 236:121795. https://doi.org/10.1016/j.matchemphys.2019.121795
9. Alazoumi SH et al (2018) Optical properties of zinc lead tellurite glasses. Resul Phys 9:1371–1376. https://doi.org/10.1016/j.rinp.2018.04.041
10. Azlan MN, Halimah MK, Umar SA, Azlina Y, El-Mallawany R, Najmi G (2018) Linear and nonlinear optical efficiency of novel neodymium nanoparticles doped tellurite glass for advanced laser glass. Educ JSMT 5(2):47–66
11. Annapoorani K, Maheshvaran K, Arunkumar S, Suriya Murthy N, Marimuthu K (2015) Structural and luminescence behavior of Er^{3+} ions doped Barium tellurofluoroborate glasses. Spectrochim Acta Part A Mol Biomol Spectrosc 135:1090–1098. https://doi.org/10.1016/j.saa.2014.08.003
12. Lakshminarayana G et al (2017) Physical, structural, thermal, and optical spectroscopy studies of TeO2–B2O3–MoO3–ZnO–R2O (R = Li, Na, and K)/MO (M = Mg, Ca, and Pb) glasses. J Alloys Compd 690:799–816. https://doi.org/10.1016/j.jallcom.2016.08.180
13. Kaur A, Khanna A, Aleksandrov LI (2017) Structural, thermal, optical and photo-luminescent properties of barium tellurite glasses doped with rare-earth ions. J Non Cryst Solids 476:67–74. https://doi.org/10.1016/j.jnoncrysol.2017.09.025
14. Kassab LRP, Courrol LC, Seragioli R, Wetter NU, Tatumi SH, Gomes L (2004) Er^{3+} laser transition in $PbO–PbF_2–B_2O_3$ glasses. J Non Cryst Solids 348:94–97. https://doi.org/10.1016/j.jnoncrysol.2004.08.132
15. Basavapoornima C et al (2017) Spectroscopic and pump power dependent upconversion studies of Er^{3+}-doped lead phosphate glasses for photonic applications. J Alloys Compd 699:959–968. https://doi.org/10.1016/j.jallcom.2016.12.199
16. Mostafa AG et al (2015) Studying the elastic properties of glasses based on Ckd using ultrasonic technique. Dig J Nanomater Biostruct 10(3):935–940
17. Abdulbaset AAA et al (2017) Effect of neodymium nanoparticles on elastic properties of zinc tellurite glass system. Adv Mater Sci Eng 2017:1–7
18. Yousef ES (2013) Er^{3+} ions doped tellurite glasses with high thermal stability, elasticity, absorption intensity, emission cross section and their optical application. J Alloy Compd J 561:234–240. https://doi.org/10.1016/j.jallcom.2013.01.199
19. Umar SA, Halimah MK, Chan KT, Latif AA (2017) Polarizability, optical basicity and electric susceptibility of Er^{3+} doped silicate borotellurite glasses. J Non Cryst Solids 471:101–109. https://doi.org/10.1016/j.jnoncrysol.2017.05.018
20. Saddeek YB (2004) Ultrasonic study and physical properties of some borate glasses. Mater Chem Phys 83:222–228. https://doi.org/10.1016/j.matchemphys.2003.09.051
21. Mustafa IS, Ain N, Razali N, Ibrahim AR, Yahaya Z, Kamari HM (2015) From rice husk to transparent radiation protection material. J Intelekt 9(2):1–6
22. Ahmad AF, Zulkifly A, Abdul Halim S, Suzan JO, Umar SA (2018) Synthesis, thermal, dielectric, and microwave reflection loss properties of nickel oxide filler with natural fiber-reinforced polymer composite. J Appl Polym Sci 135:1–10. https://doi.org/10.1002/app.46998
23. Raju CN, Babu R, Babu AM (2019) Investigation on physical, structural and optical properties of Er^{3+}—doped bismuth borate glasses for optical fiber amplifier applications. J Emerg Technol Innov Res 6:1. https://doi.org/10.1729/journal.19547
24. Azlan MN, Halimah MK, Suriani AB, Azlina Y, Umar SA, El-mallawany R (2019) Upconversion properties of erbium nanoparticles doped tellurite glasses for high efficient laser glass. Opt Commun 448:82–88. https://doi.org/10.1016/j.optcom.2019.05.022
25. Rodriguez O et al (2016) Characterization of silica-based and borate-based, titanium-containing bioactive glasses for coating metallic implants. J Non Cryst Solids 433:95–102. https://doi.org/10.1016/j.jnoncrysol.2015.09.026
26. Ali AA, Rammah YS, Shaaban MH (2019) The influence of TiO_2 on structural, physical and optical properties of

B_2O_3–TeO_2–Na_2O–CaO glasses. J Non Cryst Solids 514:52–59. https://doi.org/10.1016/j.jnoncrysol.2019.03.030
27. Rammah YS, Ali AA, Abdelghany AM (2018) Optical properties of bismuth borotellurite glasses doped with $NdCl_3$. J Mol Struct. https://doi.org/10.1016/j.molstruc.2018.07.071
28. Azlan MN, Halimah MK, Hajer SS, Suraini AB, Azlina Y, Umar SA (2019) Enhanced optical performance of tellurite glass doped with samarium nanoparticles for fiber optics application. Chalcogenide Lett 5:215–229
29. Chinnamat W, Laopaiboon R, Laopaiboon J, Pencharee S, Bootjomchai C (2017) Influence of ionic radius modifying oxides on the elastic properties of glasses using ultrasonic techniques and FTIR spectroscopy. Phys Chem Glass Eur J Glass Sci Technol Part B 58(5):207–216. https://doi.org/10.13036/17533562.58.5.101
30. Gouraud F, Chotard T, Karray R (2015) Structural, mechanical and optical investigations in the TeO_2-rich part of the TeO_2–GeO_2–ZnO ternary glass system. Solid State Sci 40:20–30. https://doi.org/10.1016/j.solidstatesciences.2014.12.009
31. Marzouk SY, Gaafar MS (2007) Ultrasonic study on some borosilicate glasses doped with different transition metal oxides. Solid State Commun 144:478–483. https://doi.org/10.1016/j.ssc.2007.09.017
32. Halimah MKK et al (2019) Study of rice husk silicate effects on the elastic, physical and structural properties of borotellurite glasses. Mater Chem Phys 238:121891. https://doi.org/10.1016/j.matchemphys.2019.121891
33. Sidek HAA, Rosmawati S, Talib ZA, Halimah MK, Halim SA (2013) Effect of zinc on the elastic behaviour of (TeO_2) 90 (AlF_3) 10-x (ZnO) x glass system. Int J Basic Appl Sci 90(09):41–44
34. Poor HB, Aziz HA, Zamiri R (2013) Ultrasonic and optical properties and emission of Er^{3+}/Yb^{3+} doped lead bismuth-germanate glass affected by Bi^{+}/Bi^{2+} ions. J Lumin 143:526–533. https://doi.org/10.1016/j.jlumin.2013.05.053
35. Greaves GN, Greer AL, Lakes RS, Rouxel T (2011) Poisson's ratio and modern materials. Nat Mater 10(11):823–837. https://doi.org/10.1038/nmat3134
36. Properties E (2007) Elastic properties and short-to medium-range order in glasses. J Am Ceram Soc 90(10):3019–3039. https://doi.org/10.1111/j.1551-2916.2007.01945.x
37. Rouxel T, Ji H, Hammouda T, Moréac A (2008) Poisson's ratio and the densification of glass under high pressure. Phys Rev Lett 100(22):1–4. https://doi.org/10.1103/PhysRevLett.100.225501
38. Hasnimulyati L, Halimah MK, Zakaria A, Halim SA, Ishak M (2017) A comparative study of the experimental and the theoretical elastic data of Tm^{3+} doped zinc borotellurite glass. Mater Chem Phys 192:228–234. https://doi.org/10.1016/j.matchemphys.2017.01.086
39. Saddeek YB, Elsayed NZ (2015) Structural and mechanical features of some lanthanum tellurite glasses. Can J Phys 93(4):460–465. https://doi.org/10.1139/cjp-2014-0044
40. Saddeek YB, El Latif LA (2004) Effect of TeO^2 on the elastic moduli of sodium borate glasses. Phys B Condens Matter 348(1–4):475–484. https://doi.org/10.1016/j.physb.2004.02.001
41. El-mallawany R (1999) Tellurite glasses Part 2. Anelastic, phase separation, Debye temperature and thermal properties. Mater Chem Phys 60:103–131
42. Zaid MHM, Matori KA, Abdul Aziz SH, Zakaria A, Ghazali MSM (2012) Effect of ZnO on the physical properties and optical band gap of soda lime silicate glass. Int J Mol Sci 13(6):7550–7558. https://doi.org/10.3390/ijms13067550
43. Rajesh S, Saravanan S, Palani R (2015) Structural and elastic properties of Li^{+} and W^{6+} metal ions doped with sodium borate glass using pulser—receiver technique. Int J Sci Res 2015:298–301
44. Saddeek YB (2005) Elastic properties of Gd 3 + -doped tellurovanadate glasses using pulse-echo technique. Mater Chem Phys 91:146–153. https://doi.org/10.1016/j.matchemphys.2004.11.005
45. Shelby JE (2005) Introduction to glass science and technology, 2nd edn. New York State College of Ceramics at Alfred University School of Engineering, Royal Society of Chemistry, Alfred, NY, USA
46. Laopaiboon R, Laopaiboon J, Pencharee S, Nontachat S, Bootjomchai C (2016) The effects of gamma irradiation on the elastic properties of soda lime glass doped with cerium oxide. J Alloys Compd 666:292–300. https://doi.org/10.1016/j.jallcom.2016.01.098